frontiers in Materials

ORIGINAL RESEARCH
published: 06 August 2019
doi: 10.3389/fmats.2019.00187

Hierarchical Twinning Induced Texture Weakening in Lean Magnesium Alloys

Indranil Basu[1]* *and Talal Al-Samman*[2]

[1] *Laboratory of Metal Physics and Technology, Department of Materials, ETH Zürich, Zurich, Switzerland,* [2] *Institut für Metallkunde und Metallphysik, RWTH Aachen University, Aachen, Germany*

Rolled and annealed Mg-1wt. %Zn-1wt. %Gd-0.6wt. %Zr (ZEK110) alloys were subjected to room temperature in-plane compression along the rolling direction, followed by isochronal annealing treatments for 1 h. Despite a starting orientation favoring c-axis extension, the as-deformed microstructure revealed a hierarchical network of twins with profuse quantities of second and third generation twinning appearing within primary tension and compression twins. Complex twin-twin and twin–particle interactions were accompanied by the activation of both basal and non-basal dislocation slip in the neighborhood. While the population density of twins nucleated was significantly high, twin growth was severely retarded due to the presence of secondary phases. In terms of the overall distribution of grain orientations, the as-deformed texture displayed a rather weak basal component with a large portion of the basal poles aligned toward the longitudinal direction with an angular spread of ± 30°. Recrystallization commenced within twins, at twin-twin intersections at lower annealing temperatures and occurred additionally near secondary phases at higher annealing temperatures, giving rise to diverse orientations of both basal and off-basal character. Subsequent growth led to favorable coarsening of the off-basal orientations resulting in an overall texture weakening. The findings provide critical insights with respect to engineering high-strength, high-ductility lean magnesium alloys, comprising hierarchical microstructures that are not only associated with favorable crystallographic textures but additionally display a multi-scale strengthening behavior.

Keywords: magnesium, twinning, twin-particle interactions, hierarchical microstructures, twin-twin interactions

OPEN ACCESS

Edited by:
Hajo Dieringa,
Helmholtz Centre for Materials and Coastal Research (HZG), Germany

Reviewed by:
Jing Su,
Max-Planck-Institut für Eisenforschung GmbH, Germany
Kristian Mathis,
Charles University, Czechia
Dong Jie,
Shanghai Jiao Tong University, China

***Correspondence:**
Indranil Basu
indranil.basu@mat.ethz.ch

Specialty section:
This article was submitted to Structural Materials, a section of the journal Frontiers in Materials

Received: *23 May 2019*
Accepted: *22 July 2019*
Published: *06 August 2019*

Citation:
Basu I and Al-Samman T (2019) Hierarchical Twinning Induced Texture Weakening in Lean Magnesium Alloys. Front. Mater. 6:187. doi: 10.3389/fmats.2019.00187

INTRODUCTION

Designing high-strength and high-cold-formability magnesium alloys remains a considerable challenge owing to the inherent anisotropy in the hexagonal crystal structure, wherein strain accommodation along the longer c-axis is difficult owing to significantly larger critical resolved shear stresses in this direction (Yoo, 1981; Mordike and Ebert, 2001; Hirsch and Al-Samman, 2013; Wu and Curtin, 2015; Wang et al., 2018). Present magnesium alloys thus show limited plasticity at ambient temperatures, primarily due to: (i) an insufficient number of active deformation mechanisms, which are unable to fulfill the von Mises criterion for homogeneous plastic deformation, and (ii) the consequent development of strong crystallographic textures during deformation giving rise to highly anisotropic plastic flow behavior (Yoo, 1981; Hirsch and Al-Samman, 2013; Wu and Curtin, 2015).

Over the past decade, there has been a focused emphasis laid upon utilizing a combination of intelligent alloying such as micro-additions of rare earth (RE) elements and optimizing microstructural design in order to obtain simultaneous strength—ductility enhancement (Bohlen et al., 2010; Al-Samman and Li, 2011; Noble, 2012; Peng et al., 2012). In this regard, the authors have previously shown the beneficial impact of combined additions of RE and non-RE elements on shear banding and, subsequent recrystallization and grain growth behavior in Mg alloys (Basu and Al-Samman, 2014). They reported that tailored microstructures displaying large ductility without any strength loss could be fabricated by appropriate thermo mechanical processing. They also inferred that the presence of non-RE elements such as Zn and Zr significantly augment the RE effects in the alloy (Basu and Al-Samman, 2014). In a similar line, the authors performed exhaustive investigations on the deformation twinning behavior in binary magnesium-rare earth alloys, wherein it was shown that the addition of solute rare earth elements modify the overall twinning response with comparable nucleation probabilities of both extension and compression twins. The impact of such twinning characteristics was evident on the annealing response that resulted in soft deformable textures devoid of the unfavorable basal texture component for industrial processing, such as sheet metal forming (Basu and Al-Samman, 2015).

Despite the significant progress made in the previous studies, there is a current lack of understanding of twinning in these systems in the presence of combined additions of RE and non-RE elements, wherein simultaneous solute as well as precipitate effects on the deformation twinning response can be exploited for an enhanced knowledge of these alloy systems. The current work thus extends our understanding of twinning characteristics in Mg-RE alloys with additional contribution from non-RE elements i.e., Zn and Zr and whether such RE—non-RE combinations can be utilized to design high strength-high ductility twinned microstructures.

BACKGROUND

Room temperature deformation of conventional Mg alloys typically offers only four independent slip deformation modes i.e., two each from the basal: (0001) $<11\bar{2}0>$, and prismatic: $(10\bar{1}0)$ $<11\bar{2}0>$ slip systems. However, since the aforementioned deformation modes only provide strain accommodation along the basal plane, magnesium tends to exhibit abundant deformation twinning activity as a strain accommodation mechanism along the <0001> c-axis (Yoo, 1981). However, unlike slip that is spatially more homogeneous with gradual lattice rotations, twinning results in drastic reorientation of the crystal by a significantly large misorientation angle (Yoo, 1981; Yoo and Lee, 1991; Aydiner et al., 2009). Such crystallographic rotation leads to formation of well-defined twin boundaries. While the presence of twin boundaries promote strengthening through dynamic grain refinement as well as lead to substantial latent hardening inside the twins; their role in terms of ductility is often seen as unfavorable (El Kadiri and Oppedal, 2010; Qiao et al., 2017). This is owing to the fact that twinning can either give rise to regions of severe shear incompatibility near the twin-parent interface (such as for compression twins) or generate crystallographically hard orientations (in case of extension twins) that adversely affect the overall elongation response (Aydiner et al., 2009; Molodov et al., 2014, 2017; Basu and Al-Samman, 2015). In this regard, promoting twin formation is often avoided when it comes to designing ductile Mg alloys, resulting in employing alternative routes such as designing fine-grained microstructures thereby abating twinning activity and increasing slip contribution (Yamashita et al., 2001; Hofstetter et al., 2015; Lin et al., 2016; Trang et al., 2018).

However, it must be understood that the aforementioned shear incompatibility and generation of non-deformable orientations during twinning is primarily as a result of the highly anisotropic dislocation slip prevalent in pure Mg, wherein pyramidal <c+a> slip modes require extremely high stresses (nearly 100 times the critical resolved shear stress of basal <a> slip) to activate (Yoo, 1981; Tonda and Ando, 2002; Wu and Curtin, 2015; Wu et al., 2018). In other words, the main reason behind the poor ductility response of twinned Mg alloys is the lack of homogeneity of slip deformation. A closer look into the origins of such poor formability indicates that the degree of anisotropy in stacking fault energies of the basal and non-basal planes plays a critical role in determining the overall plasticity response. Theoretically, the generalized stacking fault energy (γ_{GSFE}) for a crystallographic plane varies over the relative shear induced displacement that corresponds to displacing a plane of atoms by a magnitude equal to the Burgers vector. The resultant γ_{GSFE} curve along the slip direction of a crystallographic plane is described by a local maximum viz. $'\gamma_{unstable}'$ and a local minimum referred to as $'\gamma_{stable}'$. Physically, the value of $\gamma_{unstable}$ relates to the ease of generation of stacking faults on the plane i.e., dislocation nucleation and the value of γ_{stable} gives a measure of the mobility of the nucleated dislocations on the particular plane. The lower the γ_{GSFE} values, the easier is the strain accommodation on a particular crystallographic plane. In pure Mg and conventional Mg alloys, it has been shown that the stacking fault energy values of the pyramidal planes ($\gamma_{GSFE(Pyr.)}$) are larger than those for the basal planes ($\gamma_{GSFE(Bas.)}$), whereby dislocation nucleation on pyramidal planes becomes energetically unfavorable (Wu and Curtin, 2015; Wu et al., 2018). Moreover, even if they nucleate the high γ_{stable} values ensures that the glissile pyramidal dislocations immediately cross-slip to the basal planes thereby dissociating into a sessile <c> and <a>-type dislocations (Ahmad et al., 2018, 2019). By means of molecular dynamics simulations, it has been shown that the cross-slip barrier for pyramidal to basal transition is extremely low i.e., of the order of 0.3–0.5 eV (Wu and Curtin, 2015), in comparison to the cross-slip energy barrier between pyramidal planes that is calculated in the range of 0.6–0.9 eV (Ahmad et al., 2018), thereby explaining the favorability of such a transformation. In a later study, it was shown by means of atomistic simulations that addition of solute REs can contribute toward reducing the cross-slip energy barrier differential between pyramidal-pyramidal and pyramidal-basal planes by

simultaneous strengthening of basal dislocations and lowering the stacking fault energies for non-basal planes. It was further predicted that the RE-effect on ductility would be enhanced in the presence of lean additions (within 1 wt. %) of solute Zn. This ensures a more homogeneous deformation response of RE containing Mg alloys (Wu et al., 2018).

In light of these theories, it becomes interesting to probe deformation twinning in lean magnesium-rare earth alloys as a parameter for designing microstructures that benefit from twin induced strengthening without suffering in terms of reduced ductility, owing to a more isotropic slip behavior. In particular, the impact of RE additions in the presence of additional non-RE elements on the twinning response as well as the slip behavior needs to be investigated.

EXPERIMENTAL METHODS

Mg-1Gd-1Zn-0.6Zr (wt.%) alloy (ZEK110) was cast as per ref. (Basu and Al-Samman, 2014) and hot-rolled to a final thickness reduction of 50% over multiple passes. In between each pass, the alloy was subjected to intermediate annealing treatments at 450°C for a duration of 10 min. Rolling resulted in preferential alignment of the basal planes parallel to the rolling direction, giving rise to a well-defined sheet texture. The alloy was subsequently subjected to a short recrystallization annealing treatment at 400°C for only 12 min in order to relieve the stored residual stresses in the microstructure, yet retain the rolling texture for the subsequent in-plane compression experiments. The annealing treatment resulted in an average grain size of $16.7\,\mu m \pm 2.9\,\mu m$.

Specially oriented specimens of dimensions 12 mm (Longitudinal Direction; LD) × 10 mm (Transverse Direction; TD) × 4 mm (Compression Direction; CD) were machined from the rolled and heat treated sheet and utilized for in-plane compression tests, such that the compression axis is aligned with the rolling direction. Plane strain deformation conditions were implemented by means of a channel-die setup integrated into a conventional screw-driven ZWICK testing machine. Frictional shear between the specimen and the channel-die walls was mitigated by using hexagonal boron nitride (hBN) powder as a lubricant. Since the primary motivation behind such a deformation set-up was to activate deformation twinning in the material, the final compressive strain was limited to a value: $\varepsilon_{logarithmic} \sim 6\%$, which typically corresponds to the value where twinning is known to exhaust and further deformation ensues primarily by dislocation slip. In order to assess the recrystallization and grain growth related texture and microstructural evolution, the deformed microstructures were subjected to isochronal annealing treatments for 60 min at 350 and 450°C.

Microstructural characterization was performed using visible light microscopy and electron backscatter diffraction (EBSD) analysis. Specimen surface was prepared by mechanical grinding and polishing techniques, followed by final step electro-polishing, giving rise to a damage free surface. Metallographic etching was performed using acetic picral. X-ray diffraction (XRD) measurements were performed to characterize the macro texture. For this, a Bruker D8 Advance diffractometer, equipped with a high-resolution area detector, operating at 30 kV and 25 mA, using filtered iron radiation and polycapillary focusing optics was used. The measurements were performed on the specimen mid-plane to obtain the bulk texture and avoid any surface effects. The quantitative texture analysis toolbox MTEX (Hielscher and Schaeben, 2008) was employed to calculate the orientation distribution function (ODF) and visualize the data from the pole figure measurements. EBSD measurements performed on electro-polished specimens were analyzed using commercially available EBSD analysis software and the MTEX toolbox. A step size of 0.3 μm and a camera binning of 4 × 4 was employed for the measurements.

RESULTS AND DISCUSSION

Flow Behavior Under In-plane Compression

Plane-strain compression (PSC) experiments in the present work was ideally designed to generate extension along the c-axis, since it is well-known that pure Mg undergoes $\{10\bar{1}2\}$ extension twinning under such circumstances. **Figure 1** displays the averaged stress-strain curve recorded for six individual in-plane compression tests on ZEK110 alloy. The error bars indicate the range of deviation in the stress values corresponding to the imposed strain. An inset image near the top left indicates flow curves recorded for higher strains clearly elucidating the twinning onset and exhaustion regimes. The bottom right inset image in **Figure 1** indicates the (0002) basal pole figure corresponding to the starting orientation. As depicted, the basal poles though preferentially aligned toward the LD, exhibit a large angular spread around the longitudinal axis of approx. ± 15° from the CD toward the TD. This is indicated by a rather weak rolling texture of the order of ∼3 MRD (multiples of a random distribution).

The loading curve displays a "concave-up" shape that is often associated with twinning dominated deformation (Kelley and Hosford, 1968; Nave and Barnett, 2004). The initial "non-linearity" observed in the flow curves is often seen in PSC stress-strain curves and is possibly a result of compliance effects between the plunger of the channel-die and the sample. Twinning initiation is indicated with the onset of plateau and the subsequent rise in the applied stress most likely corresponds to exhaustion of twinning deformation and the corresponding twin boundary induced hardening effects (c.f. arrows shown in **Figure 1**).

Microstructure and Texture Evolution

Figures 2A,B show the optical microstructures and XRD bulk textures for ZEK110 after 6% PSC deformation and annealing at 350 and 450°C for 60 min, respectively. Despite the imposed c-axis extension, the contribution of {1012} extension twins seemed severely abated with respect to the XRD pole figure shown for the as-deformed ZEK110 alloy. Theoretically, twinning under c-axis extension is associated with an 86° reorientation of the basal poles such that they align with the

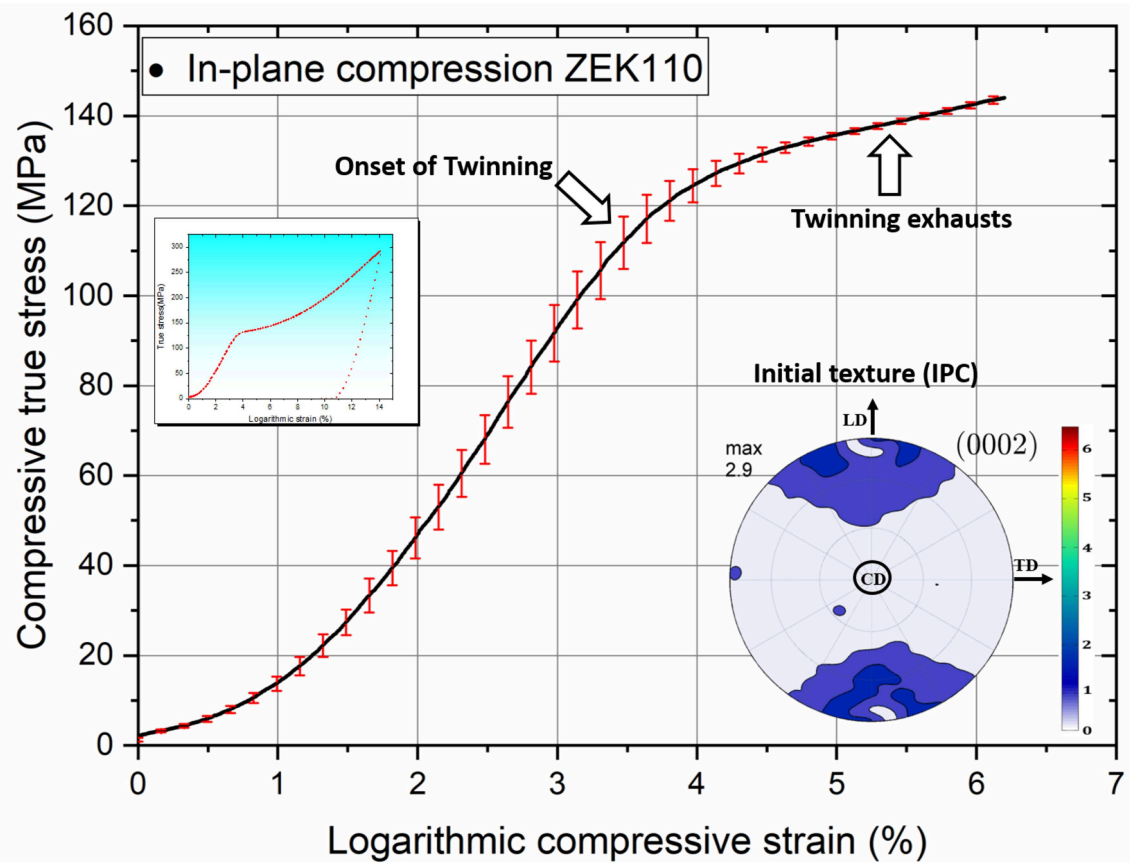

FIGURE 1 | Flow curves during in-plane compression of Mg-1wt.%Zn-1wt.%Gd-0.6wt.%Zr (ZEK110) alloy. White arrows indicate the onset of twinning and the strain at which twinning exhausts. Inset image on the lower right showing the starting texture of the specimen. Error bars indicate the stress variation across flow curves recorded for six independent deformation tests.

direction of loading i.e., CD. However, the as-deformed texture of ZEK110 displays a concentration of the basal poles lying between CD and LD, within an angular distance of $\sim 15 - 30^{\circ}$ away from the LD. Annealing treatment at 350°C results in large orientation spread between the LD and CD, weakening the overall texture intensity from 6 MRD in the as-deformed state to 4 MRD in the annealed one. Further increase in the annealing temperature to 450°C, results in complete disappearance of the basal texture component that was visible in the as deformed and lower annealing temperature conditions. The orientations mostly lay within LD and CD with an angular spread of $\pm$ 30°. The texture intensity was further weakened with the maximum value dropping to 3 MRD.

Light microscopy investigations indicated heavily twinned microstructures in the as-deformed condition. Annealing at 350°C led to a partially recrystallized microstructure comprising of equiaxed grains as well as twinned regions. At higher annealing temperatures, a combination of large and small grain clusters describe the whole grain topology. Secondary phases, identified in earlier works as Zr-rich clusters (Basu and Al-Samman, 2014), are additionally observed as heterogeneously distributed all throughout the microstructure (c.f. **Figures 2B**, **3**). It must be noted that Gd was existing entirely in solid solution in the microstructure. The size ranges vary from particles being larger than 1 μm (ideal for stimulating recrystallization) to small ones that are $< 1\,\mu$m (contribute toward grain boundary pinning; Humphreys and Hatherly, 2004).

Hierarchical Twinning and Non-basal Slip

In order to assess the characteristics and nature of deformation twins as well as the associated dislocation sub-structure generation, in depth EBSD analysis was employed to obtain simultaneously topological, orientation and strain information. **Figure 4A** shows the overall strain distribution in the as-deformed ZEK110 alloy by means of a kernel average misorientation (KAM) map. The black regions correspond to the unindexed areas and they systematically correspond to the Zr rich secondary phases present in the microstructure. The KAM physically describes the misorientation of a reference pixel i.e., kernel center, with respect to the nearest neighbor pixels lying in the defined kernel size. Since the degree of location crystal lattice rotation is directly proportional to the local shear strain, the KAM map also represents the local strain distribution in the microstructure. In the present case, a threshold KAM value of 2°

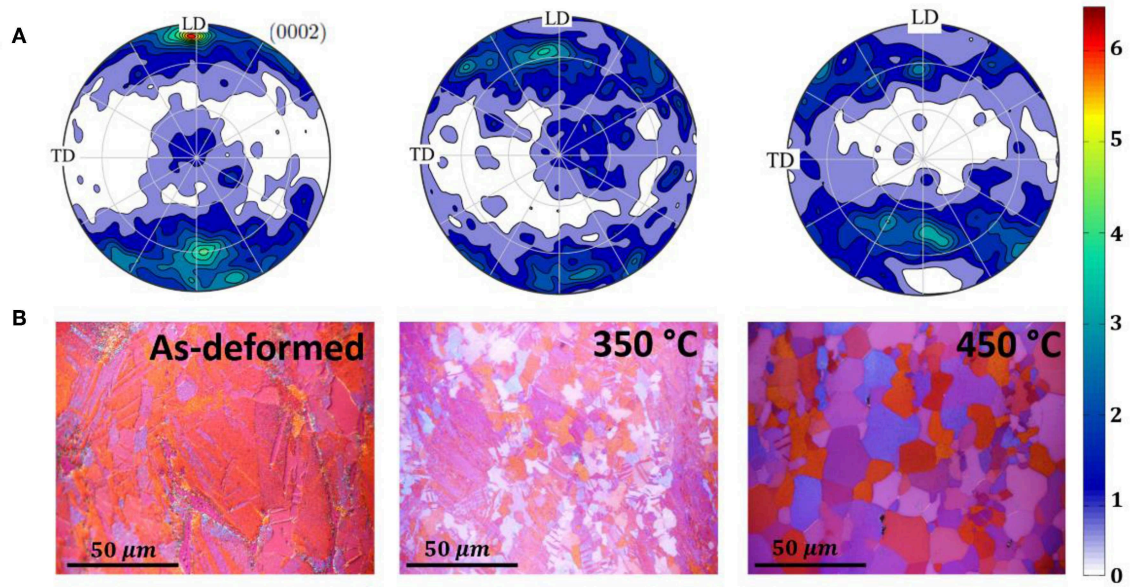

FIGURE 2 | (0002) recalculated pole figures from XRD **(A)**, and optical microstructures **(B)** after plane strain compression to 6% true strain, and static annealing treatments for 60 min at 350 and 450°C for ZEK110.

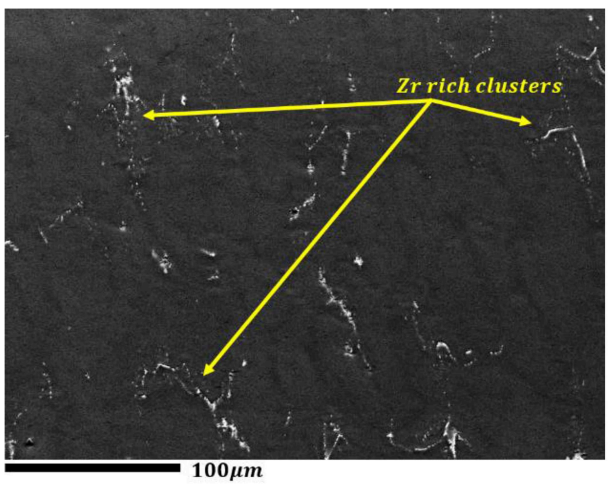

FIGURE 3 | Precipitate characterization and distribution in the ZEK110 alloy in the as-deformed state; the precipitates compositionally confer with Zr-rich phases that have been previously identified in Basu and Al-Samman (2014).

was implemented for a kernel size upto the 2nd nearest neighbor (Basu et al., 2017). **Figure 4B** displays the image quality map with grain boundaries overlaid with the definite twin axis/angle misorientation relationships. In this respect, the indexed twin boundaries in different colors revealed $\{10\bar{1}2\}$ extension twins (highlighted in red), $\{10\bar{1}1\}$ compression twins (blue) as well as $\{10\bar{1}1\} - \{10\bar{1}2\}$ double twins (yellow). An angular deviation of $\pm 6^{\circ}$ in the misorientation was accounted for. **Figure 4C** provides a magnified KAM map for the highlighted region in **Figure 4A**, depicting a strong KAM contrast. The local strain appears to systematically accumulate along slip bands (colored bright green) that correspond to $\{11\bar{2}2\}$ pyramidal <c+a> slip traces as corroborated by the image quality map shown as an inset image on the top left corner of **Figure 4C**. **Figure 4C** also reveals that the observed slip bands originate primarily near the detected $\{10\bar{1}1\} - \{10\bar{1}2\}$ double twin. The other inset of an inverse pole figure (IPF) map, with the viewing axis along the CD, indicates in-grain orientation gradients involving rotation of the $\{11\bar{2}2\}$ plane parallel to the plane of compression (c.f. yellow colored matrix in the IPF map in **Figure 4C**), thereby corroborating the existence of pyramidal <c+a> dislocation activity.

While grain boundaries play a critical role in terms of defect nucleation sites, there contribution as obstacles to dislocation motion directly influences the ease of plasticity and the degree of material strengthening that has been frequently addressed as the Hall-Petch effect. However, it must be understood that the strengthening potential of a grain boundary is strongly dependent upon the nature of dislocation-grain boundary interaction, whereby the grain boundary can (i) either act as an impenetrable barrier to dislocation motion (no transfer) leading to dislocation pile-ups and localized rotations or (ii) facilitate complete transfer of slip between two neighboring grains. This aspect is strongly influenced by the dislocation character as well as the grain boundary crystallography. A geometrical assessment of the feasibility of dislocation transfer across grain boundaries can be described via the slip transfer parameter (m') value, given as: $m' = (\mathbf{n_1} \cdot \mathbf{n_2}) \times (\mathbf{b_1} \cdot \mathbf{b_2})$, where $\boldsymbol{n_1}$ and $\boldsymbol{n_2}$ are the normalized intersection lines common to the active slip planes and the boundary plane, and $\boldsymbol{b_1}$ and $\boldsymbol{b_2}$ are the normalized slip directions in the pile-up and emission grains (Shen et al., 1988; Clark et al., 1992). While the first expression on the right hand side corresponds to the alignment of the slip planes, the

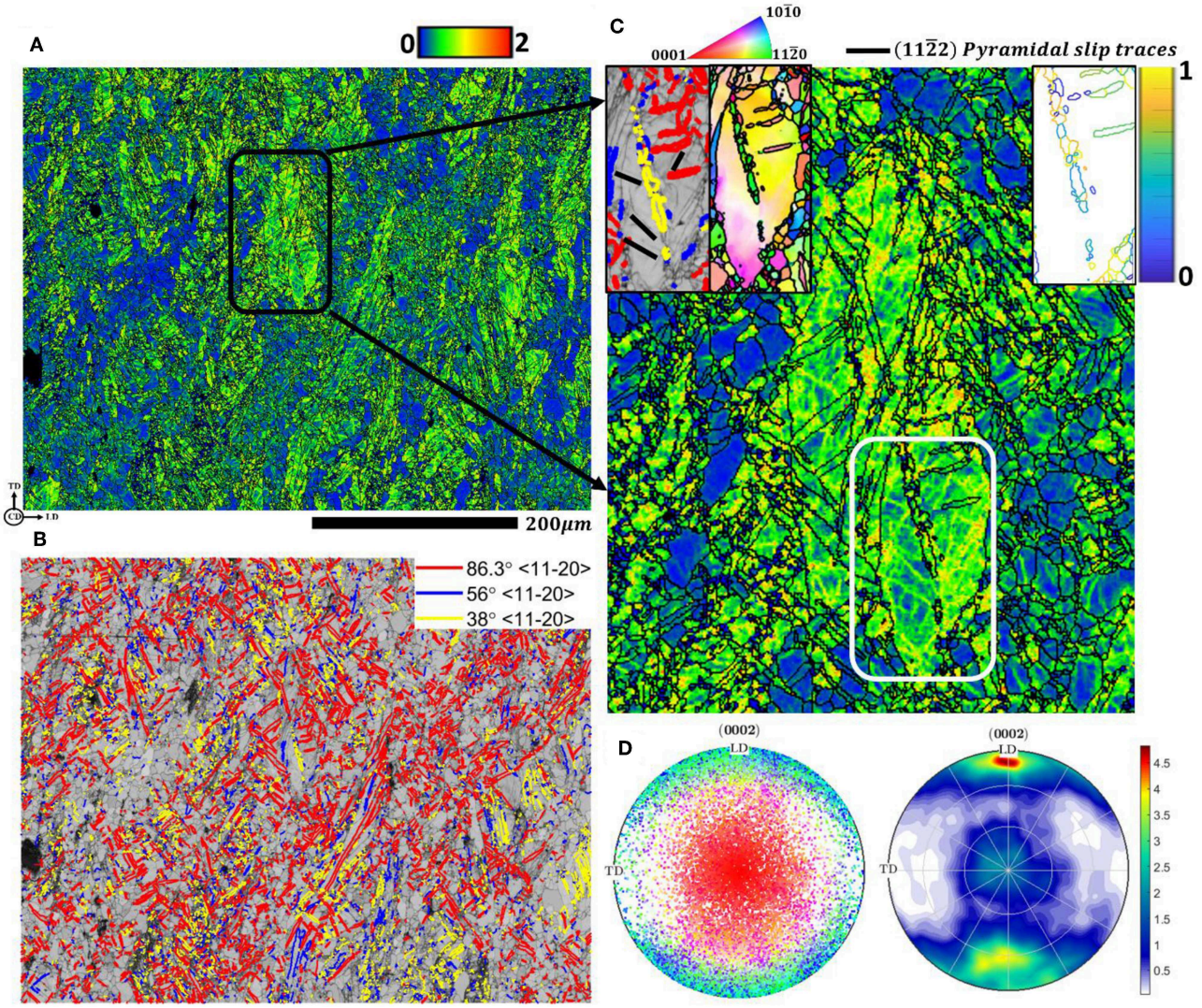

FIGURE 4 | (A) Kernel average misorientation map corresponding to ZEK110 deformed to 6% strain under plane strain compression, **(B)** corresponding image quality map with twin boundaries as $\{10\bar{1}2\}$ extension twins (highlighted in red), $\{10\bar{1}1\}$ compression twins (blue) as well as $\{10\bar{1}1\} - \{10\bar{1}2\}$ double twins (yellow); **(C)** magnified image of the area highlighted in this figure. Corresponding inverse pole figure map as inset on the top left corner and the map showing the grain boundaries colored with respect to the degree of transparency to $(11\bar{2}2) < 11\bar{2}3 >$ pyramidal slip transmission. Red lines overlaid on the map confer with $(11\bar{2}2)$ pyramidal slip traces. Grain boundaries larger than 3° are shown in black. **(D)** (0002) single orientation scatter data and recalculated pole figures for the EBSD map shown in **(A)**.

second expression is related to the alignment of the incoming and outgoing slip directions. The higher the m' value, the easier is the slip transfer, and obviously, the lower is the stress concentration and dislocation pile-up at the boundary. The inset map on the top right corner in **Figure 4C** displays grain boundaries colored with respect to the corresponding m' values calculated for $\{11\bar{2}2\}$ pyramidal <c+a> slip system as the active slip mode. Bright yellow and greenish yellow colors indicate easier slip transmission, while dark blue colored boundaries resist slip transfer i.e., block dislocation motion across the boundary. Large segments of the double-twin/parent interface in **Figure 4C** being primarily highlighted by green-yellow and yellow colors indicate that slip transfer of <c+a> dislocations across the twin boundary is geometrically favorable. The implications of such observations on the plasticity behavior in lean magnesium-rare earth alloys will be discussed later.

Apart from the presence of extension twins, in-plane compression also resulted in considerable amounts of compression twinning and higher order twin structures appearing throughout the microstructure. The likelihood of appearance of compression twins can be attributed to the larger spread of orientations about the LD, whereby certain grain orientations can experience c-axis compression arising from the lateral compressive stresses due to the die walls (Basu and Al-Samman, 2015, 2017). Moreover, the presence of pyramidal slip (as seen in **Figure 4C**) could also lead to dynamic

reorientation of the parent grains during straining, whereby parts of the grains in due course start experiencing a compressive stress component along c-axis from the loading direction. The second aspect regarding the ease of nucleation of compression twins is attributed to the presence of Gd and Zn as solutes. On one hand, addition of solute REs facilitate the reduction of overall stacking fault energies of higher order planes such that nucleation of compression twin faults becomes relatively easier (Li and Ma, 2009; Sandlöbes et al., 2012), whereas on the other side the co-segregation and formation of Zn-Gd dimers (Nie et al., 2013) could effectively increase the activation energy of atomic shuffling processes that dictate tensile twin formation. Infact, similar observations were reported for Mg-Y alloys, wherein retarded atomic shuffling in $\{10\bar{1}2\}$ extension twins was attributed to the larger shuffling energies owing to the bigger Y atoms in the matrix (Stanford et al., 2015). Both these factors have been seen to result in competitive nucleation stresses for both $\{10\bar{1}2\}$ extension and $\{10\bar{1}1\}$ compression twin formation.

A more peculiar aspect that is evident during deformation of the current alloy is the appearance of higher order twinned structures i.e., hierarchical twin formation, whereby numerous instances of 3rd generation twins are observed. **Figure 5** illustrates different cases of such hierarchical twinning observed in the as deformed ZEK110. The parent grain in **Figure 5A** exhibits all three twin types i.e., extension, compression, and double twins. The double twins additionally undergo $\{10\bar{1}2\}$ extension twinning giving rise to two different twin variants shown in red ($TT1_{DT_{1P}}$) and green ($TT2_{DT_{1P}}$). In conventional Mg alloys, the red twin corresponds to the high Schmid factor variant and the green twin is associated with the low Schmid factor variant. The former shows a higher chance of nucleating primarily due to anisotropy in slip behavior in pure Mg, wherein strain accommodation is easier for the red twins in comparison to the green twins (Basu and Al-Samman, 2015). However, the appearance of both twin variants in rather equal proportions evinces to a non-Schmid twinning behavior prevalent in the present alloy that most likely arises from more homogeneous deformation behavior. In case of **Figure 5B**, a large compression twin (CT_P) is shown to undergo both extension (TT_{CT_P}) as well as compression twinning (CT_{CT_P}). The broad non-twin like morphology of the primary compression twin (CT_P) in **Figure 5B** develops from slip-induced coalescence of large number of individual compression twins nucleating adjacent to each other, indicated by the white arrows in the image on the left (c.f. **Figure 5B**). The 2nd generation compression twin (CT_{CT_P}) further twins under a non-zero tensile stress component along the c-axis to give rise to a double twin relationship with the parent compression twin (DT_{CT_P}).

Figure 6 shows another region comprising 3rd generation twins, wherein a compression twin $'CT'_{DT_P}$ forms inside a double twin $'DT'_P$ (c.f. **Figure 6A**). Interestingly, since the twins rotate the crystal about the same $< 11\bar{2}0 >$ axis, the formation of compression twin inside a double twin results in creation of a new interface that is misoriented with respect to the original parent grain (P) by 13 about the $<11\bar{2}0>$ axis (c.f. misorientation profile along AB in **Figures 6B,E**). **Figure 6C** shows the grain-reference orientation- deviation (GROD) map corresponding to the same region, indicating large orientation gradients next the grain boundary from where the higher order compression twin seems to nucleate. **Figure 6D** displays the single orientation scatter data indicating the appearance of diverse orientations due to the formation of complex twinning structures within the same parent grain.

Using the kernel average misorientation data, the local geometrically necessary dislocation density values corresponding to the primary slip can be calculated using the strain gradient approach (Kubin and Mortensen, 2003; Konijnenberg et al., 2015) given as: $\rho_{GND} = \frac{2\theta}{n\lambda}|\boldsymbol{b_d}|$, where, θ is the experimentally measured KAM value, λ is the step size (in the present case 300 nm), n is the number of nearest neighbors averaged in the KAM calculation (in the current case 2nd nearest neighbor) and $\boldsymbol{b_d}$ is the Burgers vector corresponding to the primary slip direction, which in the current case is attributed to basal <a> slip. The GND values corresponding to <c+a> slip are estimated by performing a crystallographic decomposition of the Nye tensor obtained from the local lattice curvature values extracted from EBSD (Nye, 1953; Field et al., 2005; Ruggles and Fullwood, 2013; Konijnenberg et al., 2015). The Nye tensor ($\propto_{ij}$) describes the contribution to geometrically necessary dislocation content from multiple slip systems that are needed to accommodate a given rotation in the crystal lattice and is mathematically expressed as, $\propto_{ij} = \sum_m \rho^m \boldsymbol{b}_i^m \boldsymbol{z}_j^m$, $\boldsymbol{b}_i^m$ and $\boldsymbol{z}_j^m$ are Burgers vector and slip plane normal for slip system m and ρ^m is dislocation content for the slip system m. The variation of the 2D–GND values for both <a> and <c+a> slip are represented in **Figure 6F**. Corresponding GND maps for both basal and pyramidal slip are indicated to the right of the plot in **Figure 6F**. The values indicate only an order of magnitude difference in dislocation density values between basal <a> and pyramidal <c+a> slip near the grain boundary (c.f. calculated GND density gradient along line $'\mathbf{1-2}'$ shown in **Figure 6C** and bottom image in **Figure 6F**). It is worthwhile to mention that the GND values from the strain gradient and lattice curvature approaches provide a lower bound estimate since it incorporates the contributions of only non-paired edge dislocation segments and dislocation walls, which result in an effective unclosed burgers circuit giving rise to a net non-zero misorientation. Moreover, experimental 2D EBSD data can provide only 5 terms of the Nye tensor viz. $\propto_{ij}$. This implies that dislocation densities from a maximum of five independent dislocation systems can be resolved, whereas the effective set size of available slip systems in a hexagonal close packed material is 21, indicating that above approach underdetermines the complete dislocation content from individual slip systems. It is expected that a more accurate estimate of GND values feasible from 3D data sets would therefore lead to much higher densities that directly correlate to large local internal stresses that contribute to twin nucleation. However, the current values provide a qualitative estimate of the dislocation density contributions from basal and non-basal slip modes. The ease of non-basal <c+a> slip further elucidates the preferred nucleation of compression type

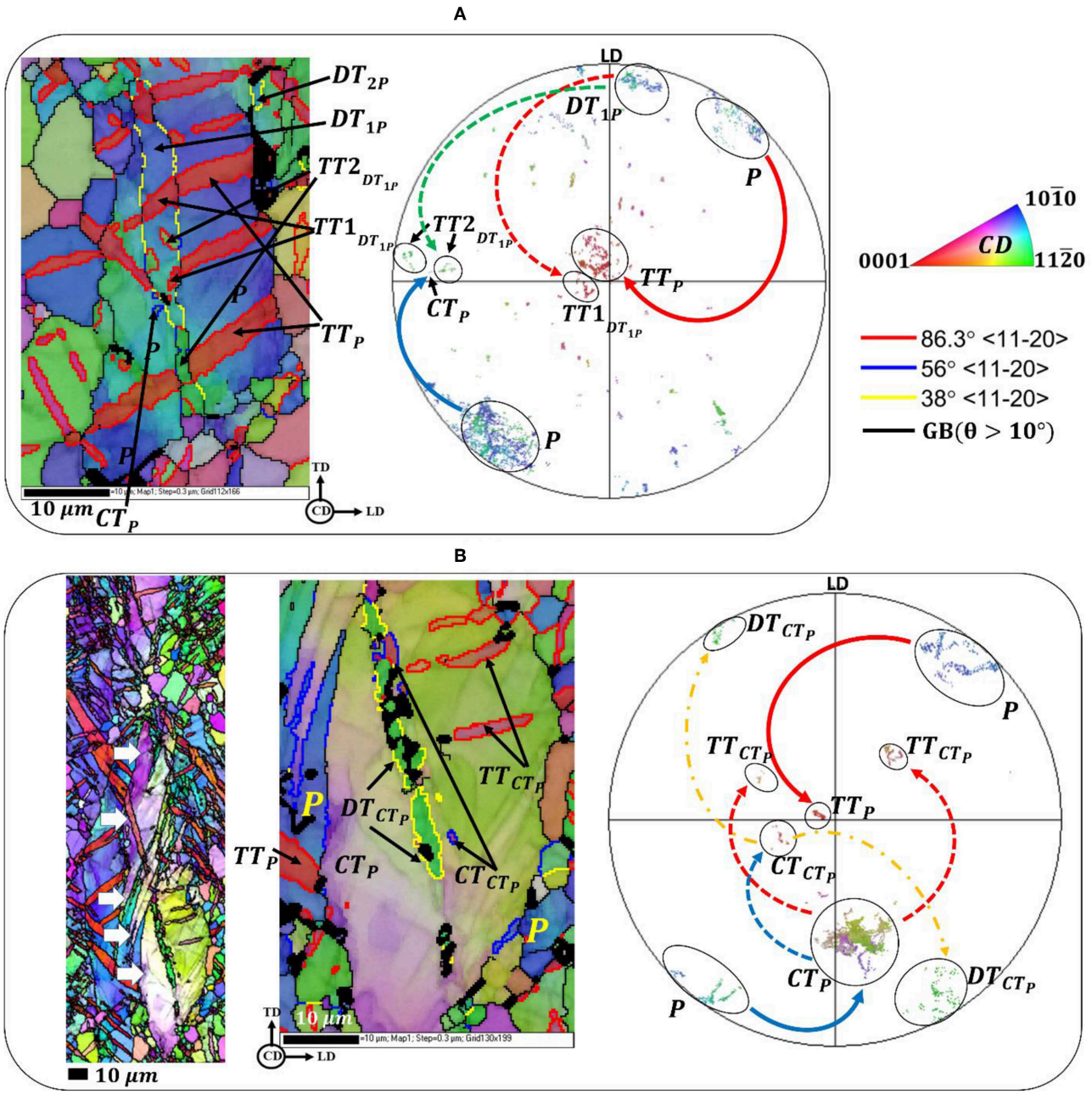

FIGURE 5 | Inverse pole figure maps and corresponding single orientation scatter data indicating different instances of hierarchically twinned structures comprising nested twins in ZEK110. The colored arrows in the single orientation scatter plots indicate the crystallographic rotation of the parent grains because of twinning. Grain boundaries larger than 10 are highlighted in black. Twin boundaries are shown as $\{10\bar{1}2\}$ extension twins (highlighted in red), $\{10\bar{1}1\}$ compression twins (blue) as well as $\{10\bar{1}1\} - \{10\bar{1}2\}$ double twins (yellow). White arrows in left most image in **(B)** indicate the remnant sections of individual compression twins that nucleated next to each other and coalesce through dislocation slip to form a broad compression twinned region.

twinning rather than formation of extension twins, which are typically the most favored twin type in pure Mg. In terms of microstructural design, it is proposed that such hierarchically twinned microstructures are extremely beneficial in terms of designing high strength-high ductility microstructures, wherein twin induced grain fragmentation results in simultaneous grain refinement, and generation of new and diverse orientations (c.f. as shown in the single orientation scatter plots and the IPF maps in **Figure 5**).

The existence and stability of such higher order twins in the current alloy are attributed to: (i) interaction of second phase particles with twins and (ii) local dislocation activity.

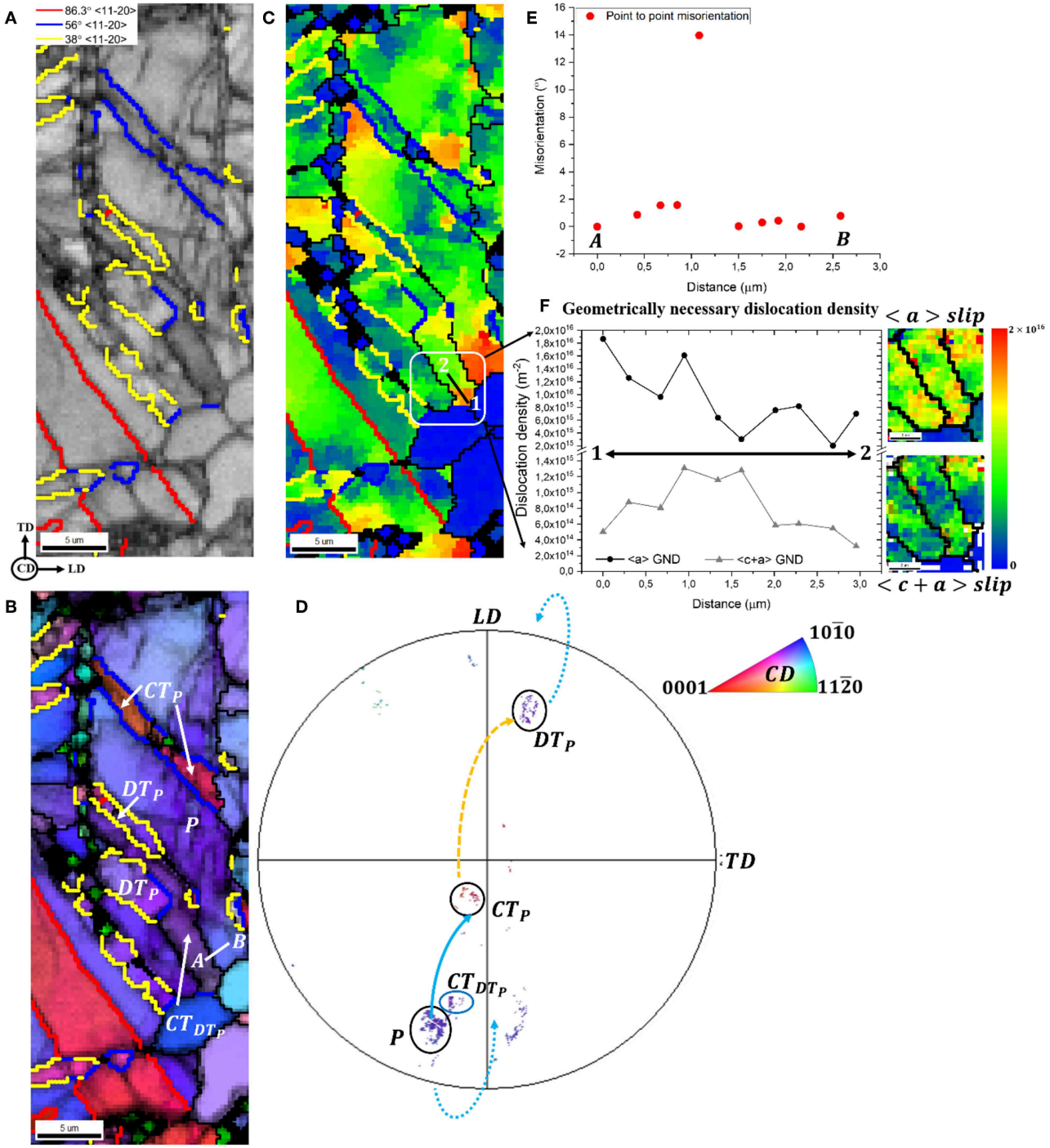

FIGURE 6 | (A) Image quality, **(B)** inverse pole figure, and **(C)** grain reference orientation deviation maps, showing formation of hierarchically twinned structures described by a {10$\bar{1}$1} compression twin nucleating inside {10$\bar{1}$1} – {10$\bar{1}$2} double twin. **(D)** Single orientation scatter data indicating the twin induced reorientations; **(E)** misorientation profile across the boundary (line AB) between the 3rd generation compression twin and the original parent grain; **(F)** geometrically necessary dislocation density gradients for <a>-type and <c+a> type slip near the grain boundary along line *1–2* are plotted as a function of distance; basal and pyramidal dislocation density maps are additionally shown to the right of the plot.

While Zr rich particles can retard twin growth severely, they also generate very high local stress states that can facilitate twin nucleation (Basu and Al-Samman, 2015). Quite contrarily, such high local stresses in pure Mg would typically result in crack nucleation rather than twins, primarily due to the large anisotropy in slip behavior. **Figure 7** shows the number of

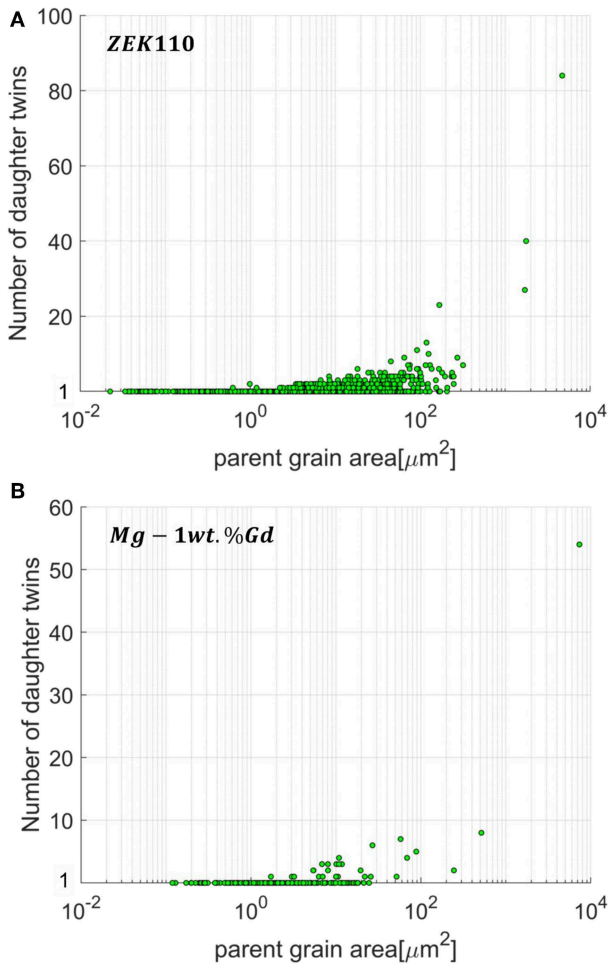

FIGURE 7 | Number of first generation twins per parent as a function of grain size for **(A)** ZEK110 and **(B)** Mg-1Gd from Basu and Al-Samman (2017).

daughter twins per grain as a function of the grain size for the ZEK110 alloy vis-a-vis solid solution Mg-1Gd alloy under the same deformation conditions. The trends indicate much higher overall twin number densities in the quaternary alloy with the number of twins nucleated in the largest grains being 1.5 higher than in the binary counterpart. The plot further indicates that the majority of the grains measured in the ZEK110 alloy nucleated multiple twins as opposed to most grains in the binary Mg-1Gd alloy comprising of only one daughter twin. It must be noted that the number of twins detected per grain in **Figure 7** only accounts for first generation twins, wherein the parent and twinned region can be distinctly identified. It is expected that the presence of more complex higher order twin structures would indicate that the realistic values of twin number density would be much higher than that measured. Nevertheless, the findings clearly address the dominance of twin nucleation in the quaternary alloy.

In order to accommodate the local strains around the twinned regions in the ZEK 110 alloy the role of dislocation slip is critical, wherein anisotropic slip behavior dominated by basal <a> slip can adversely affect local plasticity by creating regions of large strain incompatibility in and around such hierarchical twinned structures that would typically promote failure. However, the presence of non-basal dislocation activity in the present alloy can overcome this issue and effectively sustain material ductility. **Figures 8A,B** indicate microstructural regions in the as-deformed state showing abundant non-basal slip activity. In order to simultaneously visualize local orientation as well as strain distribution, EBSD maps are depicted as inverse pole figure maps overlaid upon image quality maps. The regions of lower image quality correspond to formation of slip bands inside the grains. Regions comprising such slip bands are separately identified in **Figure 8A** and magnified to reveal the character of dislocation slip active in the as-deformed state (c.f. Reg. I, Reg. II, and Reg. III in **Figure 8A**). The slip traces corresponding to $\{11\bar{2}2\}$ pyramidal planes are overlaid on the images in black lines indicating that the slip band orientations marked by black arrows are associated with 2nd order pyramidal <c+a> slip. Since pyramidal slip possesses five independent deformation modes as opposed to basal <a> slip that offers only two independent slip systems, the overall grain and twin co-deformation becomes much more homogeneous in the presence of <c+a> slip activity. This is validated by the large fraction of yellow and green colored grain boundaries, favoring pyramidal slip transfer across parent-twin interfaces (c.f. **Figures 8A,B**). On the other hand grain boundary strain transfer map for basal slip transfer indicates more blue colored boundaries (as shown in the basal <a> slip transfer map for the parent-twin interface enclosed in **Figure 8B**), thereby indicating that the same parent-twin interface can act as a strong barrier to the motion of basal <a> dislocations, shown by purple arrows. The corresponding local strain distribution (KAM map) shows larger local misorientations (higher strains) at the parent-twin interface (see lower right inset image in **Figure 8B**) that most likely corresponds to pile-up of basal dislocations at the twin boundary. The findings further indicate that while non-basal <c+a> slip contributes to enhanced plasticity, the activation of basal slip facilitates strengthening by piling-up at the newly formed parent-twin interfaces, thereby giving rise to a twinning induced dynamic Hall-Petch effect.

Recrystallization and Grain Growth Behavior

Figure 9 presents the EBSD analysis for annealing microstructure corresponding to heat treatment at 350°C for 60 min. **Figure 9A** indicates that the microstructure is partially recrystallized, highlighted by a distribution of recrystallized grains as well as still deformed regions comprising of non-recrystallized tension twins (boundaries highlighted in red). **Figure 9B** displays the corresponding (0002) pole figure. The EBSD texture indicates good agreement with the macro texture measured using XRD. In order to assess the contributions of the recrystallized and non-recrystallized grains to the overall orientation distribution, the EBSD map was classified into recrystallized (RXed) and un-recrystallized (un-RXed) areas.

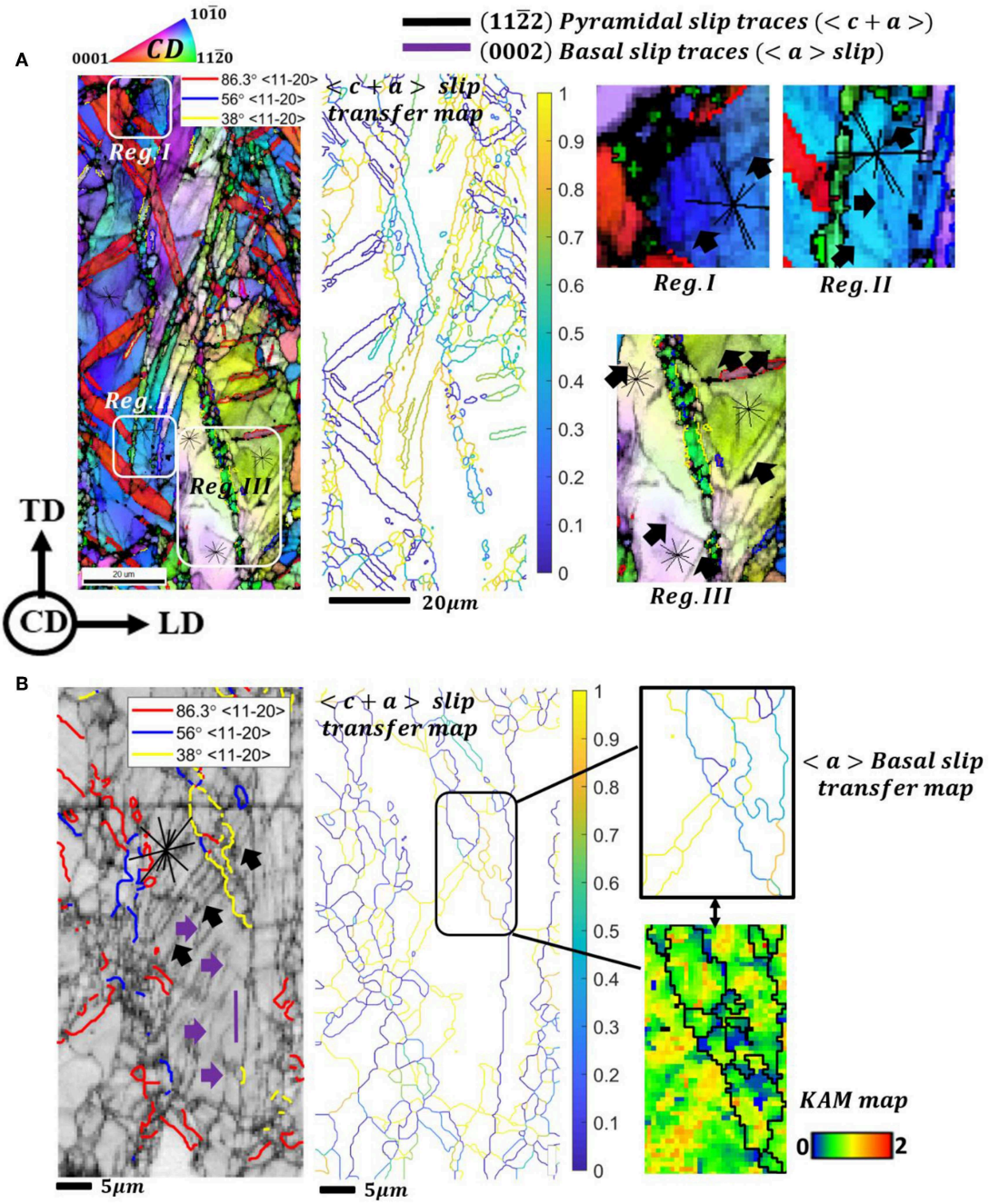

FIGURE 8 | Microstructural regions shown as inverse pole figure maps and grain boundary slip transmission map, **(A,B)** in the as-deformed ZEK110 alloy showing profuse $(11\bar{2}2) < 11\bar{2}3 >$ pyramidal slip (indicated by black slip traces) and secondary $(0001) < 11\bar{2}0 >$ basal slip (shown in purple slip traces) both inside the parent as well as twinned areas. Regions in **(A)** are magnified, indicating a good agreement of the observed slip traces in matrix and twinned regions with $(11\bar{2}2) <11\bar{2}3>$ pyramidal slip. The grain-boundary slip transfer maps in **(A,B)** correspond to $(11\bar{2}2) <11\bar{2}3 >$ pyramidal slip. The slip transmission map on the right hand side in **(B)**, describes the favorability of transfer of $(0001) <11\bar{2}0 >$ basal dislocations across the twin/grain boundaries in the region of interest highlighted by the black window. The bottom right image in **(B)** depicts the kernel average misorientation (KAM) map of the area of interest.

Figure 9C displays the recrystallized and non-recrystallized regions of the microstructure. RXed grains were characterized with a grain orientation spread (GOS) value within 2 and simultaneously possessing a grain boundary misorientation larger than 10°. The corresponding single orientation scatter plots for the RXed and un-RXed subsets are shown as inset on the top-left corner. The orientation spread indicates a higher density of orientations lying between the LD and CD for the recrystallized subset. These orientations typically correspond to those generated by compression twins and higher order twins,

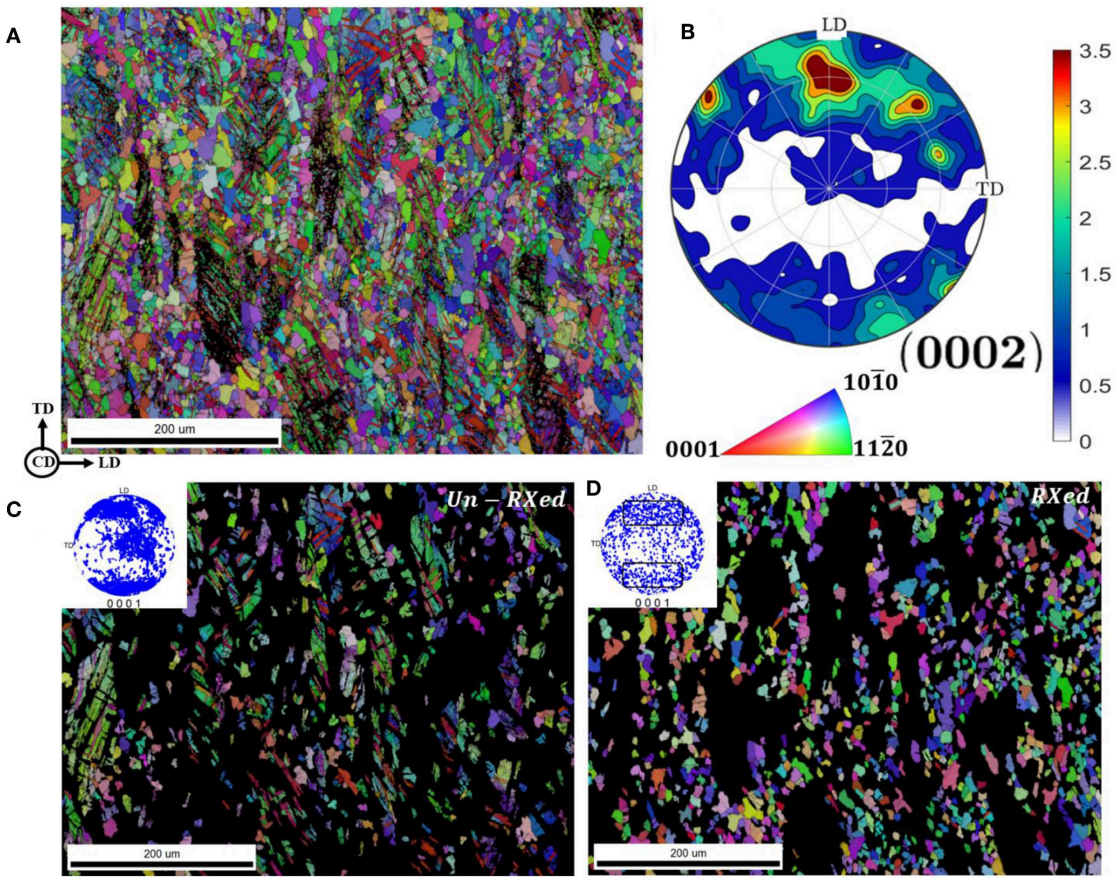

FIGURE 9 | EBSD map at 350°C (60 min annealing time) indicating a partially recrystallized microstructure, **(A)** inverse pole figure map, **(B)** recalculated (0002) pole figure, **(C,D)** show the recrystallized and un-recrystallized subsets. Corresponding single orientation scatter for recrystallized and un-recrystallized regions are shown as inset plots on the top left corner.

indicating that the compression and higher generation twins recrystallize earlier owing to larger local stored energy. This is quite likely attributed to more active <c+a> slip in the regions that are required to accommodate local strains arising from twin formation. Pyramidal slip activity near twins is critical for nucleation of compression twinning as its formation is shear dominated i.e., twin formation is driven by glide of twinning disconnections, in comparison to extension twins, where twin propagation and growth occurs primarily by atomic shuffling (Li and Zhang, 2014; Basu and Al-Samman, 2015). Presence of <c+a> slip with a Burgers vector $'\boldsymbol{b}'$ much larger than those of basal deformation modes not only increases the local stored dislocation energy ($E_{dis} \propto G\boldsymbol{b}^2$) but also provides a non-planar dislocation network that is necessary for generation of recrystallized nuclei/grains.

In case of the deformed subset, the orientations mostly conformed with the initial parent grains and extension twins that were still resistant to recrystallization. This is attributed to the tendency of the extension twins during deformation to grow via. atomic shuffling rather than deform by slip under applied stress, whereby dislocation activity is abated and subsequently leading to an absence of well-defined deformation substructure inside the twins that can potentially recrystallize under thermal activation. Moreover, the tendency of Zn-Gd dimers to segregate at the boundaries under thermal activation further drags the recrystallization process, whereby the twin boundaries are unable to recrystallize nor grow during annealing (Basu and Al-Samman, 2015). Apart from the extension-twinned regions, the vicinity of particles also did not show traces of recrystallization owing to insufficient thermal activation at 350°C.

Figure 10 indicates the microstructure after annealing for 60 min at 450°C. The microstructure indicates a clear bimodal grain size distribution with the presence of large grains and clusters of very small grains (c.f. **Figure 10A**) in the vicinity of certain unindexed areas that systematically correspond to the Zr-rich phases (c.f. yellow arrows in **Figure 10B**). The calculated texture from the EBSD data indicates an absence of basal orientations and majority of the grains with their c-axis aligned between the LD and CD along with a lateral spread of orientations along the TD. As mentioned previously, these orientations correspond to compression twins and higher generation twins. The findings indicate that the orientations

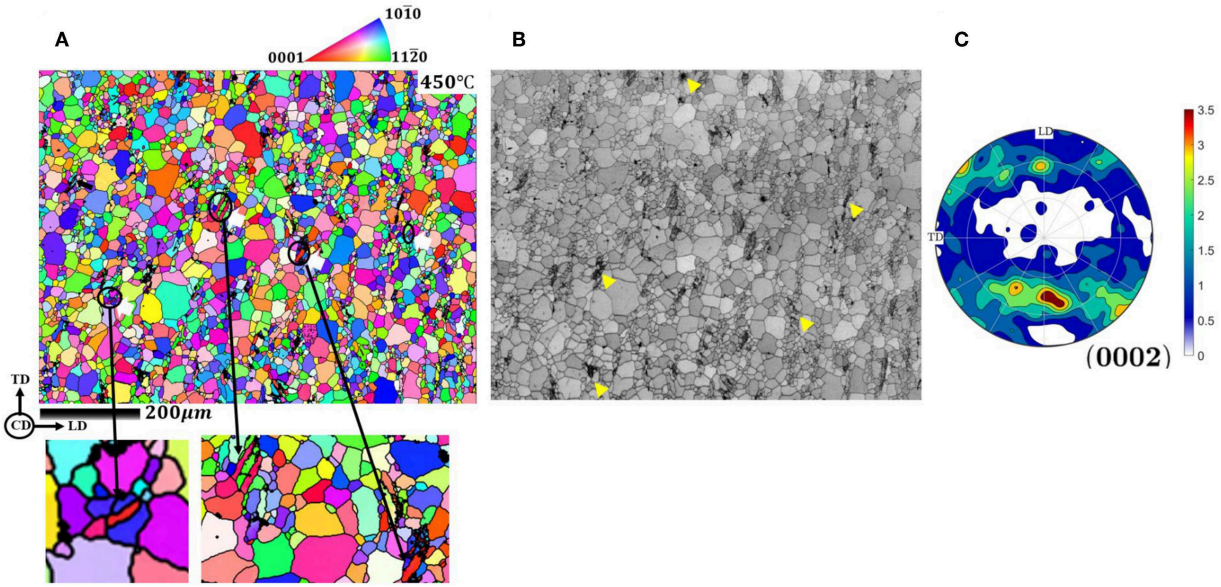

FIGURE 10 | EBSD map (at 450°C for 60 min) in inverse pole figure coloring **(A)** and image quality **(B)** color coding. Recalculated (0002) pole figure shown in **(C)**. Portions in **(A)** are zoomed in to shown the still un-recrystallized twins, marked by white arrows in **(A)**. Yellow markers in **(B)** indicate the fine grains recrystallizing near Zr-rich particle clusters.

nucleating inside the compression and higher order twins preferably undergo recrystallization and grain growth at higher annealing temperatures, thereby consuming the un-recrystallized parent grains and the majority of extension twins. Few extension twins are still visible after annealing at 450°C that seem to neither grow nor recrystallize (indicated by white arrows in **Figure 10A**). The particles generate recrystallized grains in their vicinity that give rise to the smaller grain clusters, however they seem to lack sufficient driving force to grow. The selective growth behavior in the current ZEK110 alloy is known to be an outcome of the dual effect of solute drag due to Gd-Zn solute pairs as well as Zener pinning from the finer Zr rich phases present in the microstructure (Basu and Al-Samman, 2014). The presence of such grain boundary pinning agents leads to a clear demarcation in grain sizes, wherein the smaller grains from particle stimulated recrystallization as well as extension twins possess insufficient energy to overcome the impending solute drag and particle pinning effects. On the other hand, the orientations from regions of higher stored energies are able break free of such drag effects and grow larger, subsequently dominating the overall orientation spectrum.

Implications in Terms of Microstructural Design of Lean Magnesium Alloys

The current observations are critical with respect to exploiting twinning in magnesium in order to tailor high strength-high ductility microstructures. The generic perception regarding twinning deformation in conventional Mg alloys is always associated with poor ductility response, owing to the large shear incompatibility generated near twin-parent interfaces. However, the current work reveals that through appropriate alloying strategies twinning as a deformation mode can be effectively utilized to not only accommodate imposed strain but also impart dynamic Hall-Petch strengthening.

With the means of RE-additions in conjunction with Zn and Zr, the influence of solutes as well as secondary phases on twinning behavior are favorably triggered to engineer failure resistant microstructures. From the literature, the presence of solute Zn and RE atoms contribute in intrinsically modifying basal and non-basal stacking fault energies, thereby promoting pyramidal slip as a dislocation mode as well as giving rise to a more competitive twin nucleation behavior in terms of extension and compression type twins. Simultaneously the role of Zr rich secondary phases becomes critical in severely restricting twin growth on one side and on the other hand contributing toward increasing the local stresses in the matrix to facilitate nucleation of compression twins. The superposition of both these factors contributes toward generating hierarchically twinned microstructures that not only give rise to a large orientation spread i.e., weak and deformable textures that are sustained during recrystallization and grain growth, but also promote dynamic grain fragmentation that imparts additional grain boundary hardening via. dynamic Hall-Petch mechanism.

CONCLUSIONS

Twinning induced deformation and subsequent annealing response is investigated for Mg-1wt.% Zn-1wt.% Gd-0.6wt.% Zr rolled alloy under plane strain compression perpendicular to the c-axis. It is shown that the role of non-REs can not only augment RE-solute effects on the overall deformation and annealing response but also play a significant role

as secondary phases on impacting twinning behavior. Microstructures with hierarchical twins and profuse non-basal slip are observed. The following key conclusions are derived at,

a) Plane strain compression, despite normal to the c-axis, resulted in profuse amounts of both compression and extension type twins. Large amounts of 2nd and 3rd generation twins with a hierarchical morphology are present throughout the microstructure, giving rise to simultaneous grain fragmentation and large orientation spreads.
b) Twin growth is severely restricted by the Zr rich secondary phases and on the other hand local stress states near particles and grain boundaries promote twin nucleation.
c) Nested twin structures are supplemented with abundant $\{11\bar{2}2\}$ pyramidal <c+a> slip in and around the twin-parent interfaces. While <c+a> slip accommodates the local plastic shear across the newly formed twin boundaries, basal slip tends to accumulate at the interfaces resulting in local dislocation pile-up and contributing to the overall grain boundary strengthening.
d) Recrystallization and grain growth preferentially occur inside the compression and higher order twin structures that overcome solute and particle pinning effects, whereas the recrystallized grains nucleating around particles and recovered extension twins remain pinned even at higher annealing temperatures.
e) The implications of the current study are critical with respect to exploiting twinning to design high strength-high ductility lean Mg alloys.

DATA AVAILABILITY

The datasets generated for this study are available on request to the corresponding author.

AUTHOR CONTRIBUTIONS

IB designed the study, performed the experiments, and wrote the manuscript. IB and TA-S performed the data analysis and scientific interpretation of the work and made critical revisions to the article.

ACKNOWLEDGMENTS

The financial support of the Deutsche Forschungsgemeinschaft (DFG) (AL 1343/1-2) is gratefully acknowledged. The authors are grateful for Aniruddha Dutta for his assistance in the experiments.

REFERENCES

Ahmad, R., Wu, Z., Groh, S., and Curtin, W. A. (2018). Pyramidal II to basal transformation of ⟨c + a⟩ edge dislocations in Mg-Y alloys. *Scripta Mater.* 155, 114–118. doi: 10.1016/j.scriptamat.2018.06.026

Ahmad, R., Yin, B., Wu, Z., and Curtin, W. A. (2019). Designing high ductility in magnesium alloys. *Acta Mater.* 172, 161–184. doi: 10.1016/j.actamat.2019.04.019

Al-Samman, T., and Li, X. (2011). Sheet texture modification in magnesium-based alloys by selective rare earth alloying. *Mater. Sci. Eng. A* 528, 3809–3822. doi: 10.1016/j.msea.2011.01.080

Aydiner, C. C., Bernier, J. V., Clausen, B., Lienert, U., Tomé, C. N., and Brown, D. W. (2009). Evolution of stress in individual grains and twins in a magnesium alloy aggregate. *Phys. Rev. B* 80:024113. doi: 10.1103/PhysRevB.80.024113

Basu, I., and Al-Samman, T. (2014). Triggering rare earth texture modification in magnesium alloys by addition of zinc and zirconium. *Acta Mater.* 67, 116–133. doi: 10.1016/j.actamat.2013.12.015

Basu, I., and Al-Samman, T. (2015). Twin recrystallization mechanisms in magnesium-rare earth alloys. *Acta Mater.* 96, 111–132. doi: 10.1016/j.actamat.2015.05.044

Basu, I., and Al-Samman, T. (2017). Competitive twinning behavior in magnesium and its impact on recrystallization and texture formation. *Mater. Sci. Eng. A* 707, 232–244. doi: 10.1016/j.msea.2017.09.053

Basu, I., Ocelík, V., and De Hosson, J. T. M. (2017). Measurement of spatial stress gradients near grain boundaries. *Scripta Mater.* 136, 11–14. doi: 10.1016/j.scriptamat.2017.03.036

Bohlen, J., Yi, S., Letzig, D., and Kainer, K. U. (2010). Effect of rare earth elements on the microstructure and texture development in magnesium–manganese alloys during extrusion. *Mater. Sci. Eng. A* 527, 7092–7098. doi: 10.1016/j.msea.2010.07.081

Clark, W. A. T., Wagoner, R. H., Shen, Z. Y., Lee, T. C., Robertson, I. M., and Birnbaum, H. K. (1992). On the criteria for slip transmission across interfaces in polycrystals. *Scripta Metal. Mater.* 26, 203–206. doi: 10.1016/0956-716X(92)90173-C

El Kadiri, H., and Oppedal, A. L. (2010). A crystal plasticity theory for latent hardening by glide twinning through dislocation transmutation and twin accommodation effects. *J. Mech. Phys. Solids* 58, 613–624. doi: 10.1016/j.jmps.2009.12.004

Field, D. P., Trivedi, P. B., Wright, S. I., and Kumar, M. (2005). Analysis of local orientation gradients in deformed single crystals. *Ultramicroscopy* 103, 33–39. doi: 10.1016/j.ultramic.2004.11.016

Hielscher, R., and Schaeben, H. (2008). A novel pole figure inversion method: specification of the MTEX algorithm. *J. Appl. Crystallogr.* 41, 1024–1037. doi: 10.1107/S0021889808030112

Hirsch, J., and Al-Samman, T. (2013). Superior light metals by texture engineering: optimized aluminum and magnesium alloys for automotive applications. *Acta Mater.* 61, 818–843. doi: 10.1016/j.actamat.2012.10.044

Hofstetter, J., Rüedi, S., Baumgartner, I., Kilian, H., Mingler, B., Povoden-Karadeniz, E., et al. (2015). Processing and microstructure–property relations of high-strength low-alloy (HSLA) Mg–Zn–Ca alloys. *Acta Mater.* 98, 423–432. doi: 10.1016/j.actamat.2015.07.021

Humphreys, F. J., and Hatherly, M. (2004). *Recrystallization and Related Annealing Phenomena.* Oxford, UK: Pergamon Press.

Kelley, E., and Hosford, W. (1968). Plane-strain compression of magnesium and magnesium alloy crystals. *Trans. Met. Soc. AIME* 242, 5–13.

Konijnenberg, P. J., Zaefferer, S., and Raabe, D. (2015). Assessment of geometrically necessary dislocation levels derived by 3D EBSD. *Acta Mater.* 99, 402–414. doi: 10.1016/j.actamat.2015.06.051

Kubin, L. P., and Mortensen, A. (2003). Geometrically necessary dislocations and strain-gradient plasticity: a few critical issues. *Scripta Mater.* 48, 119–125. doi: 10.1016/S1359-6462(02)00335-4

Li, B., and Ma, E. (2009). Pyramidal slip in magnesium: Dislocations and stacking fault on the {1011} plane. *Philos. Magaz.* 89, 1223–1235. doi: 10.1080/14786430902936707

Li, B., and Zhang, X. Y. (2014). Global strain generated by shuffling-dominated {1012}<1011> twinning. *Scripta Mater.* 71, 45–48. doi: 10.1016/j.scriptamat.2013.10.002

Lin, J., Wang, X., Ren, W., Yang, X., and Wang, Q. (2016). Enhanced strength and ductility due to microstructure refinement and texture weakening of the

GW102K alloy by cyclic extrusion compression. *J. Mater. Sci. Technol.* 32, 783–789. doi: 10.1016/j.jmst.2016.01.004

Molodov, K. D., Al-Samman, T., and Molodov, D. A. (2017). Profuse slip transmission across twin boundaries in magnesium. *Acta Mater.* 124, 397–409. doi: 10.1016/j.actamat.2016.11.022

Molodov, K. D., Al-Samman, T., Molodov, D. A., and Gottstein, G. (2014). Mechanisms of exceptional ductility of magnesium single crystal during deformation at room temperature: multiple twinning and dynamic recrystallization. *Acta Mater.* 76, 314–330. doi: 10.1016/j.actamat.2014.04.066

Mordike, B. L., and Ebert, T. (2001). Magnesium: properties — applications — potential. *Mater. Sci. Eng. A* 302, 37–45. doi: 10.1016/S0921-5093(00)01351-4

Nave, M. D., and Barnett, M. R. (2004). Microstructures and textures of pure magnesium deformed in plane-strain compression. *Scripta Mater.* 51, 881–885. doi: 10.1016/j.scriptamat.2004.07.002

Nie, J. F., Zhu, Y. M., Liu, J. Z., and Fang, X. Y. (2013). Periodic segregation of solute atoms in fully coherent twin boundaries. *Science* 340:957. doi: 10.1126/science.1229369

Noble, K. R. (2012). *Origins of strength and ductility in Mg-RE binary alloys*. (Doctoral dissertation). Available online at: http://hdl.handle.net/11375/11839

Nye, J. F. (1953). Some geometrical relations in dislocated crystals. *Acta Metall.* 1, 153–162. doi: 10.1016/0001-6160(53)90054-6

Peng, Q., Huang, Y., Kainer, K. U., and Hort, N. (2012). High ductile as-cast Mg–RE based alloys at room temperature. *Mater. Lett.* 83, 209–212. doi: 10.1016/j.matlet.2011.08.009

Qiao, H., Guo, X. Q., Oppedal, A. L., El Kadiri, H., Wu, P. D., and Agnew, S. R. (2017). Twin-induced hardening in extruded Mg alloy AM30. *Mater. Sci. Eng. A* 687, 17–27. doi: 10.1016/j.msea.2016.12.123

Ruggles, T. J., and Fullwood, D. T. (2013). Estimations of bulk geometrically necessary dislocation density using high resolution EBSD. *Ultramicroscopy* 133, 8–15. doi: 10.1016/j.ultramic.2013.04.011

Sandlöbes, S., Friák, M., Zaefferer, S., Dick, A., Yi, S., Letzig, D., et al. (2012). The relation between ductility and stacking fault energies in Mg and Mg–Y alloys. *Acta Mater.* 60, 3011–3021. doi: 10.1016/j.actamat.2012.02.006

Shen, Z., Wagoner, R. H., and Clark, W. A. T. (1988). Dislocation and grain boundary interactions in metals. *Acta Metal.* 36, 3231–3242. doi: 10.1016/0001-6160(88)90058-2

Stanford, N., Marceau, R. K. W., and Barnett, M. R. (2015). The effect of high yttrium solute concentration on the twinning behaviour of magnesium alloys. *Acta Mater.* 82, 447–456. doi: 10.1016/j.actamat.2014.09.022

Tonda, H., and Ando, S. (2002). Effect of temperature and shear direction on yield stress by 11$$bar 2$$2<$$overline 11 $$23> slip in HCP metals23> slip in HCP metals. *Metal. Mater. Trans. A* 33, 831–836. doi: 10.1007/s11661-002-0152-z

Trang, T. T. T., Zhang, J. H., Kim, J. H., Zargaran, A., Hwang, J. H., Suh, B. C., et al. (2018). Designing a magnesium alloy with high strength and high formability. *Nat. Commun.* 9:2522. doi: 10.1038/s41467-018-04981-4

Wang, X. J., Xu, D. K., Wu, R. Z., Chen, X. B., Peng, Q. M., Jin, L., et al. (2018). What is going on in magnesium alloys? *J. Mater. Sci. Technol.* 34, 245–247. doi: 10.1016/j.jmst.2017.07.019

Wu, Z., Ahmad, R., Yin, B., Sandlöbes, S., and Curtin, W. A. (2018). Mechanistic origin and prediction of enhanced ductility in magnesium alloys. *Science* 359:447. doi: 10.1126/science.aap8716

Wu, Z., and Curtin, W. A. (2015). The origins of high hardening and low ductility in magnesium. *Nature* 526:62. doi: 10.1038/nature15364

Yamashita, A., Horita, Z., and Langdon, T. G. (2001). Improving the mechanical properties of magnesium and a magnesium alloy through severe plastic deformation. *Mater. Sci. Eng. A* 300, 142–147. doi: 10.1016/S0921-5093(00)01660-9

Yoo, M. H. (1981). Slip, twinning, and fracture in hexagonal close-packed metals. *Metallurg. Trans. A* 12, 409–418. doi: 10.1007/bf02648537

Yoo, M. H., and Lee, J. K. (1991). Deformation twinning in h.c.p. metals and alloys. *Philos. Magaz. A* 63, 987–1000. doi: 10.1080/01418619108213931

Conflict of Interest Statement: The authors declare that the research was conducted in the absence of any commercial or financial relationships that could be construed as a potential conflict of interest.